

Radiative Electron Capture to the Continuum and the Short-Wavelength Limit of Electron-Nucleus Bremsstrahlung in 90A MeV U⁸⁸⁺(1s²2s²) + N₂ Collisions

M. Nofal,^{1,2,3} S. Hagmann,^{2,3,*} Th. Stöhlker,³ D. H. Jakubassa-Amundsen,⁴ Ch. Kozhuharov,³ X. Wang,⁵ A. Gumberidze,³ U. Spillmann,³ R. Reuschl,³ S. Hess,³ S. Trotsenko,³ D. Banas,³ F. Bosch,³ D. Liesen,³ R. Moshammer,¹ J. Ullrich,¹ R. Dörner,² M. Steck,³ F. Nolden,³ P. Beller,³ H. Rothard,⁶ K. Beckert,³ and B. Franczak³

¹Max Planck Institut für Kernphysik, D-69117 Heidelberg, Germany

²Institut für Kernphysik, Universität Frankfurt, D-60438 Frankfurt, Germany

³Gesellschaft für Schwerionenforschung GSI, D-64291 Darmstadt, Germany

⁴Mathematisches Institut, Ludwig-Maximilians-Universität, D-80333 München, Germany

⁵Modern Physics Institute, Fudan University, Shanghai 200433, People's Republic of China

⁶Centre Interdisciplinaire de Recherche Ion-Laser CIRIL, GANIL, F 14070 Caen, France

(Received 2 January 2007; published 18 October 2007)

We have measured the continuum momentum distribution for radiative electron capture to the continuum (RECC) cusp electrons in 90A MeV U⁸⁸⁺ + N₂ → U⁸⁸⁺ + {N₂^{++*}} + e_{cusp}(0°) + hν (RECC) collisions. We demonstrate that x rays coincident with RECC cusp electrons originate from the short-wavelength limit of the electron-nucleus bremsstrahlung and explain the asymmetric cusp shape by comparison with theory within the relativistic impulse approximation.

DOI: 10.1103/PhysRevLett.99.163201

PACS numbers: 34.50.Fa, 32.80.-t

Ever since Bethe [1] first calculated the electron energy distribution in the continuum following ionization and electron capture in ion-atom collisions it appeared that energy and angle differential cross sections for electron transfer provide astoundingly detailed information about the dynamics of the collision process [2–6]. The observation of a prominent cusp-shaped peak (“cusp”) at $\vec{v}_{\text{electron}} = \vec{v}_{\text{projectile}}$ in the double differential cross sections (DDCS) for electron emission pointed out a most salient feature: the key role played by the low-lying states of the projectile continuum, i.e., electrons with $\vec{v}_{\text{electron}} \approx \vec{v}_{\text{projectile}}$ in the laboratory frame and very small projectile rest frame velocity $v_{e-\text{ps}} \ll v_{\text{projectile}}$ (in the nonrelativistic approximation $\vec{v}_{e-\text{ps}} \approx \vec{v}_{\text{electron}} - \vec{v}_{\text{projectile}}$) [2].

At low collision energies, these states are populated by either nonradiative electron capture from bound states of the target (electron capture to continuum ECC) or by excitation to the continuum from bound projectile states (electron loss to continuum ELC). The prominent feature distinguishing the two cusp processes is the pronounced longitudinal asymmetry of the ECC cusp skewed to the low energy side in contrast to the near symmetric ELC cusp. The unexpected but cogent many-body features [6,7] at low collision velocity and strong perturbation have impeded so far an *a priori* theoretical understanding.

At higher velocities, far away from the range of quasi-resonance with corresponding capture probabilities $P \approx 1$, now $P \ll 1$ and kinematical considerations are of paramount importance as the two-particle electron-projectile system must lose a large amount of internal kinetic energy. At these collision energies, at few A MeV and above, a

large minimum momentum k of the order $m_e v_{\text{proj}}$ (m_e : electron mass) must be provided [8].

An entirely new perspective for the dynamics of low-lying projectile electron continua arising in heavy ion-atom collisions, i.e., the cusps, was opened when it was shown that with the collision velocity increasing and approaching the relativistic domain the radiative capture to bound and continuum channels (REC and RECC) will rapidly gain importance over the nonradiative capture channel (EC and ECC). Radiative capture exhibits a much gentler decrease with collision energy than its nonradiative counterpart because of the additional radiative degree of freedom [2,3(b),9]. In the RECC and ECC processes initial and final states are identical except for the presence of a photon appearing with the RECC.

A detailed analysis of the RECC [3(b),10] exposed the close interrelation of the radiative capture process and bremsstrahlung: the radiative capture of a loosely bound target electron into a continuum state of the heavy projectile close to threshold appears in the projectile rest frame—i.e., in inverse kinematics—as the fundamental process of electron-nucleus bremsstrahlung (eN B-S) at the short-wavelength limit, where the entire kinetic energy of the incident electron is transferred to the outgoing photon.

A similar relation between quasifree and free electron scattering via inverse kinematics is known from several other processes occurring in ion-atom and electron-atom collisions, respectively. Among them are electron loss or binary encounter electron emission and elastic electron scattering [11], as well as REC and the photoeffect [9]. Extensive theoretical investigations of the short-

wavelength region of eN *B-S* [12,13] have pointed out its relation to photoionization and its paramount importance as a precision probe for the active electron's wave function in the high *E* field very near to the projectile nucleus.

Interestingly enough, measurements of the fully differential cross section (FDCS) of the elementary process of eN *B-S* ($e, e\gamma$), which means coincident detection of *B-S* photon and the corresponding electron with well-defined vector momentum have only been possible for the low and medium energy part of the *B-S* spectra [14]. However, these pertinent experimental tests of theory could so far not be extended to the theoretically most interesting short-wavelength limit [14] as in the case of standard kinematics, i.e., an electron incident on an atom at rest in the laboratory frame, this would require coincidences between a *B-S* photon and an outgoing electron of near zero kinetic energy to determine the FDCS. By showing with the current experiment that the RECC electron corresponds to an x ray from the short-wavelength limit of eN *B-S* we emphasize that now the high electron energy resolution in the emitter frame gained from inverse kinematics—as illustrated in the RECC cusp shape—will facilitate for the first time to extend high resolution measurements of eN *B-S* all the way up to the short-wavelength limit; i.e., into a region of around the last 100 eV of the high energy tip region of the spectrum.

We also note that the current investigation is closely related to recent comprehensive studies of eN *B-S* in the domain of strong Coulomb fields of high *Z* ions [15]. They have indicated that the slope of the *B-S* continua in the vicinity of the short-wavelength limit is not entirely explained by first order Born theory.

We thus find ourselves here in a situation that in inverse kinematics, i.e., a highly charged ion as projectile incident on a quasielectron target, coincidences between electrons in the RECC cusp and bremsstrahlung photons open the door to access the long desired fully differential cross sections for the elementary process of electron-nucleus bremsstrahlung at the short-wavelength limit [10]. This step from doubly to fully differential cross sections can be accomplished once the full angular distribution of electrons in the projectile frame can be reconstructed from the RECC spectra. Then all correspondences of photoionization and eN *B-S* at the short-wavelength limit can be put to experimental scrutiny [16].

The experiment was performed at the supersonic gas target of the GSI experimental storage ring ESR as only this facility can provide high *Z* projectile beams in very high charge states *q* over a wide velocity range with the necessary brilliance [17]. Here U⁶⁵⁺ ions from the SIS synchrotron with a specific energy of 90 A MeV ($\gamma = 1.0966$, $\beta = 0.4104$, $v_{\text{proj}} = 56.24$ a.u., $p_0 = 61.67$ a.u., $E_{\text{cusp}} = 49.36$ keV) are further stripped using a thin C foil and U ions selected in charge state 88+ are injected into the ESR. Using the U⁸⁸⁺(1s²2s²) beam instead of bare

uranium in this pioneering experiment enables us to exploit the very large cross section for the ELC cusp production to conveniently facilitate tuning of the electron spectrometer during setup. Beam components undergoing charge exchange during electron cooling are intercepted by scrapers in the dipole magnet following the cooling section so that only the U⁸⁸⁺ beam traverses the N₂ gas target.

As illustrated in Fig. 1, projectiles in charge state U⁸⁷⁺ and U⁸⁹⁺, which have undergone a charge changing collision in the target zone, are detected in the first dipole magnet following the target area. X rays from the interaction volume are detected at 90° with respect to the beam axis with a HPGe x ray detector. Electrons emitted in the forward direction at $0^\circ \pm 1.9^\circ$ are separated from the coasting beam by a 60° dipole magnet downstream of the target zone. This magnet is the first optical element of the imaging forward electron spectrometer, consisting of a 60° dipole, a quadrupole triplet, and a second 60° dipole. Following momentum defining slits electrons are detected with a channel plate detector equipped with a 2D position sensitive delay line anode. The momentum resolution of the spectrometer is $\Delta p/p \approx 1.9\%$.

Relative DDCS for forward electron production are measured by incrementing the electron spectrometer's *B* fields after a predetermined number of fillings of the ESR from SIS. As functions of the electron momentum they are normalized to integrated projectiles using x rays detected with additional HPGe detectors mounted around the target area. Although we report only on DDCS a coincidence measurement is mandatory because at the chosen collision velocity the nonradiative ECC prevails [3], such that the

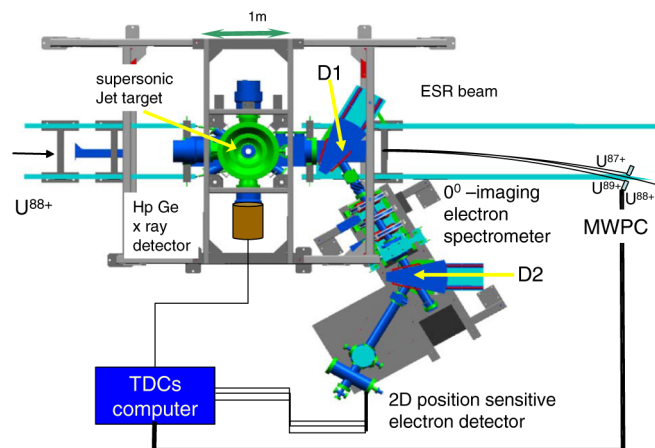


FIG. 1 (color online). Top view of the experimental setup at the supersonic jet target area of the ESR (see text). Dipole magnets D1 and D2 are indicated. Correction coils are located downstream from the target area outside the section viewed in this figure thus not affecting the measured electron spectra. Charge exchanged projectiles are detected with multiwire proportional counters MWPCs. Time signals of incoming data are analyzed using time to digital converters TDCs.

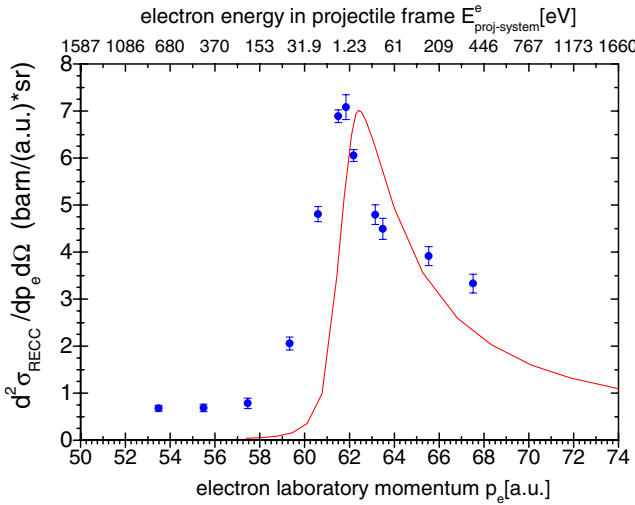
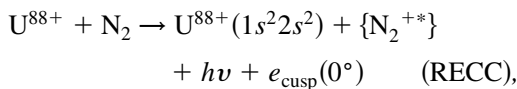


FIG. 2 (color online). RECC cusp, i.e., the double differential cross section (DDCS) for radiative electron capture to the continuum (RECC) as a function of the electron momentum in a.u. (lower scale). The abscissa on the top corresponds to the electron kinetic energy in the projectile frame $E_{\text{proj. system}}^e$. Note the highly nonlinear relation between laboratory momentum p_e and projectile frame electron energy $E_{\text{proj. system}}^e$. The full curve represents the theoretical DDCS folded with the instrumental momentum resolution. The experimental cross section is normalized to the maximum of the theoretical DDCS.

noncoincident ECC electron cusp would dominate the measured spectrum.

In Fig. 2 we show the double differential cross section for radiative electron capture to the projectile continuum, i.e., the RECC cusp, for



which has been derived as a function of the electron momentum in the laboratory frame from coincidences between x-ray photons detected under $\theta = 90^\circ$ and electrons analyzed in the forward electron spectrometer. The DDCS exhibits a cusp at $\vec{v}_{\text{electron}} = \vec{v}_{\text{projectile}}$ (i.e., $p_e/p_0 = 1$) which coincides with the simultaneously measured ELC and the ECC cusp maxima (we note that for the RECC coincidences no simultaneous coincident charge exchanged projectile was detected).

The pronounced peak asymmetry emphasizes the high energy slope of the cusp, which is well described by theory. The asymmetry is opposite to the one found for Coulomb capture (ECC) at lower collision energies [8,18]: For an observer in the U^{88+} -projectile frame the incident target electron is decelerated from $v_{e-\text{ps}} \approx v_{\text{proj}}$ to a velocity ≈ 0 , its total kinetic energy being carried away by the x-ray photon. The electron remains with very little kinetic energy $E_{\text{proj. system}}^e$ in the projectile frame, bounces back from the projectile and, thus, appears—now seen in the laboratory

reference frame—predominantly in the beam direction with corresponding momentum $p_e > \gamma v_{\text{projectile}}$ (γ = relativistic mass). Comparison is made with RECC calculations using the relativistic impulse approximation [3(b)], a convolution of the Elwert-Haug B - S theory [14] with the momentum distribution of the initial electronic state [3(b)]. The experiment is normalized to theory at the cusp maximum. The full curve in Fig. 2 represents the theoretical DDCS (with its divergence at $\vec{v}_{\text{electron}} = \vec{v}_{\text{projectile}}$) folded with the instrumental momentum resolution. The theory is integrated over the acceptance of the photon detector. Since the latter implies integration over the target Compton profile, the different subshell contributions differ at most by 5% for the high collision energy considered here.

We observe the maximum of the theoretical DDCS for RECC at a slightly higher electron laboratory momentum than the experimental maximum. In fact, this shift of the theoretical curve away from the “true” cusp position \vec{p}_0 is due to the folding procedure. The asymmetric shape function S of the theoretical DDCS with its true maximum centered at $\vec{v}_{\text{electron}} = \vec{v}_{\text{projectile}}$ is shifted into the direction of the gentler slope of S , i.e., in the direction of higher electron momenta, if folded with a resolution function R . The comparison of experimental and theoretical cusp shapes is complicated, however, by a contribution appearing in the experimental DDCS that is not accounted for by theory: It originates from electrons captured into Rydberg states of the projectile and subsequently field ionized in the 60° magnet. Such electrons have been demonstrated [19,20] to contribute significantly to the electron cusp. For a magnetic field not exceeding 40 G in the spectrometer dipole we estimate from $n = \frac{1}{2} \sqrt[4]{\frac{Z^3}{\beta \gamma C B}}$ with Z the actual

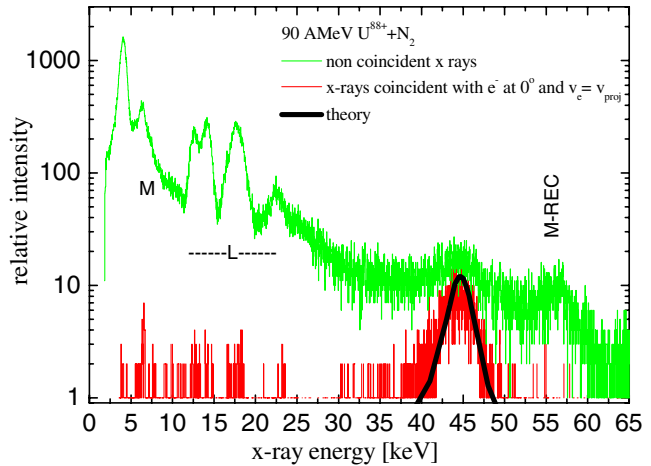


FIG. 3 (color online). X-ray spectrum coincident with RECC electrons compared with a singles, i.e., noncoincident x-ray spectrum detected at $\theta = 90^\circ$ with respect to the beam axis and with theory. The width of the x-ray peak is mainly given by the resolution function of the photon detector. The range of the characteristic U L and M x rays is indicated.

projectile charge that electrons captured into bound states with $n \geq 450$ will be field ionized. This supplemental part of the electron spectrum is centered at $\vec{v}_{\text{electron}} = \vec{v}_{\text{projectile}}$ and is not shifted by folding with R ; its inclusion in a theoretical calculation, not consistently feasible within the present approach, would tend to reduce the difference between the experimental and theoretical peak positions.

The x-ray spectra coincident with the electrons from the cusp impressively confirm the interpretation of RECC as the inverse bremsstrahlung at the short-wavelength limit (viewed by an observer in the projectile system). In Fig. 3 we compare the x-ray spectrum coincident with electrons from the cusp peak at $v_{\text{elec}} = v_{\text{proj}}$ with a noncoincident x-ray spectrum which has been scaled down for convenience of comparison. While the noncoincident spectrum is dominated by characteristic projectile M and L x-ray emission, the coincident spectrum almost exclusively contains x rays at $E_x \approx 45$ keV which coincides with the short-wavelength limit of eN $B-S$ $E = (\gamma - 1)mc^2\gamma^{-1}(1 - \beta \cos\theta)^{-1}$ from $e^- + U^{88+}$ at $(\gamma - 1)mc^2 = 49.4$ keV incident kinetic electron energy and $\theta = 90^\circ$ x-ray observation angle. Also shown is the calculated photon spectrum obtained from the fourfold differential cross section by integrating over the forward electron acceptance cone and the energy resolution of the spectrometer. Theory is normalized to experiment in the peak maximum to show the good representation of the experimental peak width by theory.

We have measured for the first time coincidences between electrons from the RECC cusp and bremsstrahlung at 90° for $90A$ MeV $U^{88+} + N_2$ collisions. We have confirmed the interpretation of RECC electrons as originating from the fundamental process of electron-nucleus bremsstrahlung at the short-wavelength limit. There is a satisfactory agreement between experiment and theory with respect to the principal features in the cusp electron and coincident photon spectra. A comparison on an absolute scale is deferred to future work. We note that with a configuration where all pertinent momenta are determined—e.g., using a reaction microscope in addition to a 2D position sensitive detector for cusp electrons,—the measurement of FDCS for the short-wavelength limit of eN $B-S$ will become feasible. This will provide an experimental test of the usual approximations made in the theoretical treatment.

We gratefully acknowledge financial support by the GSI F&E program, the BMBF, the Max Planck Gesellschaft MPG, and the DFG.

*s.hagmann@gsi.de

- [1] H. Bethe, Ann. Phys. (Leipzig) **397**, 325 (1930).
- [2] R. Shakeshaft and L. Spruch, Rev. Mod. Phys. **51**, 369 (1979).
- [3] (a) D. H. Jakubassa-Amundsen, Eur. Phys. J. D **41**, 267 (2007); (b) D. H. Jakubassa-Amundsen, J. Phys. B **36**, 1971 (2003); in the literature RECC is also called RI = radiative ionization.
- [4] A. Skutlartz *et al.*, Phys. Rev. A **28**, 3268 (1983).
- [5] H. Schmidt-Böcking *et al.*, Phys. Lett. A **122**, 421 (1987).
- [6] A. Skutlartz *et al.*, J. Phys. B **21**, 3609 (1988).
- [7] O. Jagutzki *et al.*, J. Phys. B **24**, 993 (1991).
- [8] J. Burgdörfer, *Lecture Notes in Physics* (Springer, New York, 1984), Vol. 213, p 32.
- [9] J. Eichler and Th. Stöhlker, Phys. Rep. **439**, 1 (2007).
- [10] D. H. Jakubassa-Amundsen, Radiat. Phys. Chem. **75**, 1319 (2006).
- [11] S. Hagmann *et al.*, J. Phys. B **25**, L287 (1992); E. Benis *et al.*, Phys. Rev. A **69**, 052718 (2004).
- [12] McVoy and U. Fano, Phys. Rev. **116**, 1168 (1959).
- [13] Pratt *et al.*, Phys. Rev. **120**, 1717 (1960); Phys. Rev. A **11**, 1797 (1975).
- [14] E. Haug and W. Nakel, *The Elementary Process of Bremsstrahlung*, Lecture Notes Vol. 73 (World Scientific, Singapore, 2004).
- [15] T. Ludziejewski *et al.*, J. Phys. B **31**, 2601 (1998); Hyperfine Interact. **114**, 165 (1998).
- [16] We are aware that our use of the term “fully differential” only includes kinematic parameters and disregards spin and polarization parameters which can be of considerable importance; see, e.g., S. Tashenov *et al.*, Phys. Rev. Lett. **97**, 223202 (2006).
- [17] A. Gumberidze *et al.*, Phys. Rev. Lett. **94**, 223001 (2005).
- [18] D. Jakubassa in Ref. [8], p. 17.
- [19] Z. Vager *et al.*, Phys. Rev. Lett. **48**, 592 (1982); D. Schneider *et al.*, Phys. Rev. A **34**, 169 (1986); B. DePaola *et al.*, J. Phys. B **29**, 1247 (1996).
- [20] From R. Yin *et al.*, Phys. Rev. A **36**, 1207 (1987); C. M. Lee *et al.*, Phys. Rev. A **12**, 1825 (1975); the presence of a strong REC to high n bound states may be inferred as these authors show a continuity of the cross section density for radiative capture to high n states and tip BS processes.